Environ Ecol Stat (2007) 14:207–227
DOI 10.1007/s10651-007-0016-1

Shifts in the spatio-temporal growth dynamics of shortleaf pine

Mevin B. Hooten · Christopher K. Wikle

Received: 1 March 2005 / Revised: 1 September 2005 / Published online: 10 July 2007

Abstract Previous studies focusing on the growth history of *Pinus echinata* at the edge of its geographical range have suggested that changes in growth correspond to climatic and non-climatic (e.g., anthropogenic) factors. We employ a regime-dependent state-space model that allows us to detect and characterize the changes in tree growth dynamics over space and time using readily available dendrochronological and climatic data in the presence of various sources of uncertainty. We utilize methods common in atmospheric sciences but relatively unknown in ecology and forestry to develop a hierarchical model for tree growth and describe the growth dynamics. The utility of such methods for addressing ecological problems will grow as more high dimensional spatio-temporal processes are considered and datasets become more readily available.

Keywords State-space models · Dynamical systems · Dendrochronology · Empirical orthogonal functions · Principal oscillation patterns

1 Introduction

1.1 Shortleaf pine

Due to a steady decline in shortleaf pine (*Pinus echinata*) prevalence since European settlement along the Northwest border of its natural range (Southern Missouri, Arkansas, and Eastern Oklahoma), the species has garnered much attention as it is important both economically and ecologically (Stambaugh 2001; Hamilton 2003). It has been demonstrated

M. B. Hooten (✉)
Department of Mathematics and Statistics,
Utah State University, Logan, UT 84322-3900, USA
e-mail: mevin.hooten@usu.edu

C. K. Wikle
Department of Statistics, University of Missouri,
Columbia, MO 65211, USA

that growth of shortleaf pine in this region is associated with climatic variables, especially Palmer Drought Severity Index (PDSI; Stambaugh and Guyette 2004). This does not come as a surprise since historical values of PDSI are reconstructed partially through the knowledge of tree growth during those periods (Fritts 1976). It is particularly interesting however, that Stambaugh and Guyette (2004) found the relationship between shortleaf pine growth rates and PDSI changing over time. Due to major land use changes and fire disturbance regimes in the region before and after 1880 (Cunningham and Hauser 1989; Guyette et al. 2002), it is speculated that the trees may be responding to some interaction between climatic and non-climatic factors. Information about the dynamics of growth in each one of those settings could be useful for managers wishing to promote active management of this species in the area. Shortleaf pine tree-ring data can offer insight into the changes in growth dynamics but presents numerous challenges for statistical modeling.

1.2 Dendrochronology

Dendrochronology is by no means a new science. Researchers have long been interested in the growth rates of trees over time and their relationship with other environmental and biotic variables (Fritts 1976). Dendrochronologists learn about tree growth mainly by collecting, examining, and analyzing cores from trees (Stokes and Smiley 1996). These cores are quantitatively measured based on the amount of seasonal growth evidenced by sections of denser wood (i.e., tree-rings).

Data constructed from such measurements can be thought of statistically as an individual time-series for each tree, however, generally such data are combined into one time-series representing multiple trees of the same species in a given area. These time-series are termed "chronologies". Chronologies are thought to represent the general growth dynamics of the species in a given area over very large time domains (generally hundreds of years). Therefore, they make excellent sources of data for analyses relating tree growth to climate and other environmental factors. Of course, the chronologies are constructed in the presence of many different sources of error. Measurement error in the field, measurement error in the laboratory, preprocessing error (construction of the chronologies from individual measurements), as well as spatial auto-correlation are all possible sources of uncertainty affecting the quantitative analysis of these data.

1.3 Modeling challenges

We implement a hierarchical Bayesian state-space model to estimate and assess the changes in spatio-temporal growth dynamics of shortleaf pine over a large regional area. We use readily (and publicly) available dendrochronological and climatic data to inform the model. The hierarchical framework allows us to appropriately account for the numerous sources of uncertainty at various levels and provides a natural way to intuitively model the process in a non-linear dynamical fashion. It is important to note two things; first, that this method is quite general and could be applied to other ecological and environmental processes (Beliner et al. 2000; Wikle and Royle 2007) and, secondly, that other approaches could be taken to address this problem. The methods presented here were employed because they are suited to the specific scientific application and more generally because they are underutilized in an ecological setting (owing much more popurarity to atmospheric and environmental sciences).

2 Material and methods

2.1 Data

Eight shortleaf pine chronologies were selected from three states (Fig. 1) based on the location, time period they cover, and the type of standardization applied. Location selection was limited mostly to the Ozark central hardwoods region because of the implications for specific changes in growth and management there (Stambaugh and Guyette 2004). Temporal selection was based on both the length of time period and coverage of the anthropogenically induced changepoint (year 1880). Both time criteria are critical because limited data will fail to adequately describe the dynamics in this setting. Specifically, tree-ring data from 1779 to 1977 were extracted from the eight chronologies to yield a vector time-series of dimension $n \times T$ where $n = 8$ and $T = 199$.

Standard chronologies were selected because the standardization process involves detrending, indexing, and removal of effects from endogenous stand disturbances although they are not processed using autoregressive modeling (Cook and Holmes 1986) as this would interfere with the estimation of dynamics over time. Generally the raw data are such that values (unitless tree-ring indices) over 1,000 refer to years where trees grew more than average and under 1,000 corresponds to years where tree growth was below average. Since the dynamics are of primary interest, we arbitrarily standardized the tree-ring data for convenience (i.e., subtracted the mean and divided by the standard deviation). Table 1 provides the location names and data contributors of the selected shortleaf pine chronologies meeting the above criteria.

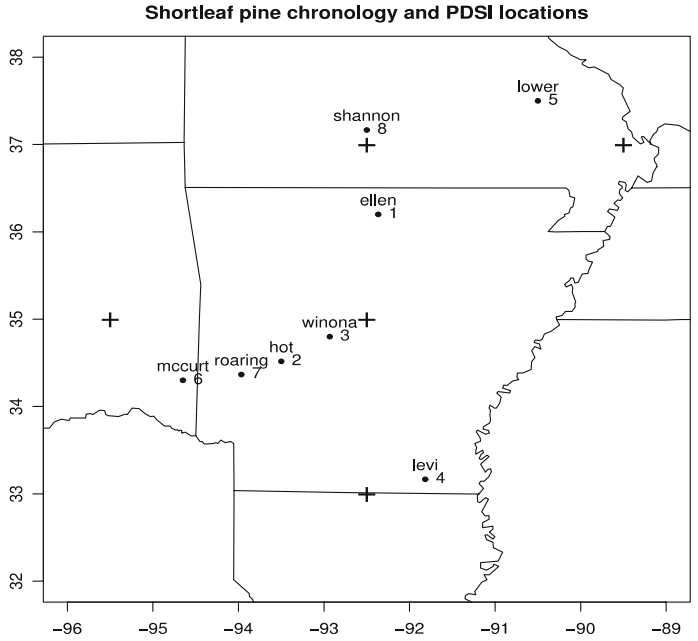

Fig. 1 Locations of *Pinus echinata* stands from which chronologies were constructed (points). Numeric values represent location in state vector. Pluses (+) denote PDSI locations

Table 1 Shortleaf pine chronology locations and contributors; order corresponds to state vector location

Name	Label	State	Contributor(s)
Ellen Cockran Hollow	ellen	Arkansas	D. Stahle
Hot Springs	hot	Arkansas	D. Stahle et al.
Lake Winona Natural Area	winona	Arkansas	D. Stahle and G. Hawks
Levi Wilcoxon	levi	Arkansas	D. Stahle and G. Hawks
Lower Rock Creek	lower	Missouri	D. Duvick
McCurtain County Wilderness	mccurt	Oklahoma	D. Stahle et al.
Roaring Branch	roaring	Arkansas	D. Stahle et al.
Shannon County	shannon	Missouri	R. Guyette

Compliments of the international tree-ring data bank (see references)

Palmer Drought Severity Index (PDSI, Cook et al. 1999) was used as a covariate in the model because of the demonstrated correlation at various times with shortleaf pine growth. A total of 5 PDSI sites spanning the region occupied by the eight chronology sites were selected (Fig. 1) for the same time period. Values were averaged over space yielding a regional PDSI covariate.

2.2 EOF analysis

Empirical Orthogonal Function (EOF) analysis (or Principal Components Analysis in the discrete setting considered here) has been used extensively in meteorological and atmospheric science to assess dominant spatial structures and their time-varying nature as well as to reduce the dimensionality of large space-time data sets common to the discipline (Preisendorfer 1988). In this setting we can apply EOF analysis to determine how the principal spatial structures in shortleaf pine growth evolve through time. This approach is well known for its optimality properties related to minimization of truncation error (Papoulis and Pillai 2002) and could be motivated more directly as a model for the spatial component of shortleaf pine growth. However, we employ it somewhat arbitrarily as a means with which to define a lower-dimensional latent process within the ecological system of interest and therefore refer the interested reader to Ash (1975) for details not provided in this paper.

Consider the following matrix formulation: Let $\mathbf{Z} = \{\mathbf{z}_1, \ldots, \mathbf{z}_t, \ldots, \mathbf{z}_T\}$ be the data matrix where each $\mathbf{z}_t$ is an $n \times 1$ vector, made up of tree-ring indices at time t for each spatial location i, where $i = 1, \ldots, n$. Then let the $n \times n$ sample lag-zero (in time) spatial covariance matrix, $\mathbf{C}_0^Z$, be decomposed using the spectral decomposition theorem:

$$\mathbf{C}_0^Z = \tilde{\mathbf{\Phi}} \tilde{\mathbf{\Lambda}} \tilde{\mathbf{\Phi}}', \tag{1}$$

where $\tilde{\mathbf{\Phi}}$ is composed of the eigenvectors ($\tilde{\boldsymbol{\phi}}_i$) and $\tilde{\mathbf{\Lambda}}$ is a diagonal matrix with the eigenvalues on the diagonal (i.e., $\tilde{\mathbf{\Lambda}} = diag(\tilde{\lambda}_i)$ for $i = 1, \ldots, n$ and $\tilde{\lambda}_1 > \ldots > \tilde{\lambda}_n$).

The eigenvectors (or principal component loadings) can then each be viewed as spatial maps representing spatial structures of the system in decreasing order of importance corresponding to the magnitude of the eigenvalues (which are decreasing and real since $\mathbf{C}_0^Z$ is positive definite). The ith spatial structure's ($\tilde{\boldsymbol{\phi}}_i$) relative importance to the system at time t can be examined by assessing the time-series resulting from a projection of the data onto the set of basis functions. In essence, EOF analysis is about assessing dominant spatial patterns in the data as well as the magnitude and frequency of their reoccurrence over time.

The expression in (1) also provides a means of reducing the dimensionality of the data. By considering only the first l eigenvectors, eigenvalues, and PC score time-series, we are

guaranteed to capture $100 \times (P_l)$ percent of the variability in the system, where $P_l = \frac{\sum_{i=1}^{l} \lambda_i}{\sum_{j=1}^{n} \lambda_j}$. Therefore, we have,

$$\mathbf{C}_0^Z \approx \mathbf{\Phi}\mathbf{\Lambda}\mathbf{\Phi}', \tag{2}$$

where $\mathbf{\Phi}$ is $n \times l$ and $\mathbf{\Lambda} = diag(\lambda_i)$, for $i = 1, \ldots, l$.

Thus, an EOF decomposition of the tree-ring data would allow us to assess dominant components of variation in the space-time system as well as allow us to model a smaller dimensional latent dynamical system. This can greatly increase computational efficiency while retaining the information contributing significantly to the variability in the system (Wikle and Cressie 1999; Beliner et al. 2000). It is important to note that atmospheric datasets are often very high dimensional, whereas most ecological datasets (due to lack of scope or inaccessibility) are possibly orders of magnitude lower dimensional. In these cases, the resulting lower dimensional system can still be advantageous as it is often decorrelated in addition to acting as a filter due to the exclusion of components contributing little to the overall variability.

2.3 Model

We adopt the now conventional hierarchical model framework as proposed by Berliner (1996) where we have a data model, process model, and parameter model. The data consist of an $n \times T$ matrix $\mathbf{Z}$ with columns corresponding to time and rows corresponding to spatial locations (i.e., different chronologies) and is modeled as a latent dynamical process ($\mathbf{y}_t$) plus error, yielding the following data model:

$$\begin{aligned} \mathbf{z}_t &= \mathbf{y}_t + \tilde{\boldsymbol{\nu}}_t + \boldsymbol{\nu}_t, \\ &= \mathbf{\Phi}'\mathbf{a}_t + \boldsymbol{\varepsilon}_t, \text{ where } \boldsymbol{\varepsilon}_t \sim N(0, \mathbf{R}), \text{ for } t = 1, \ldots, T, \end{aligned} \tag{3}$$

where $\mathbf{y}_t \equiv \mathbf{\Phi}'\mathbf{a}_t$, $\tilde{\boldsymbol{\nu}}_t$ is a non-dynamical spatio-temporal process, and $\boldsymbol{\nu}_t$ corresponds to measurement error. We will retain the compact matrix notation as in (3) for convenience throughout the remainder of the paper, however, summation notation illustrates the simplicity of the model:

$$y_{j,t} = \sum_{i=1}^{l} \phi_{i,j} a_{i,t} + \varepsilon_{i,t} \text{ for } t = 1, \ldots, T \quad \text{and} \quad j = 1, \ldots, n,$$

where $\mathbf{y}_t = [y_{1,t}, \ldots, y_{n,t}]'$, $\mathbf{\Phi}' = [(\phi_{i,j})]_{n \times l}, \forall i, j$, and $\mathbf{a}_t = [a_{1,t}, \ldots, a_{l,t}]'$. The $\phi_{i,j}$ are assumed known and the $a_{i,t}$ will be modeled hierarchically. This clarifies the separation between temporal and spatial components (in $\mathbf{y}_t$).

Here we assume that the underlying (i.e., latent) dynamical system ($\mathbf{y}_t$) lies on some lower-dimensional manifold, relative to the observed data. That is, the dynamics of shortleaf pine growth in this region can be adequately described by fewer than $n = 8$ components, say l components, where $l < n$, given by $\mathbf{a}_t$. Therefore, $\tilde{\boldsymbol{\nu}}_t$ can be thought of as an error associated with the truncation of basis functions from the spectral decomposition (e.g., Wikle and Cressie 1999) and $\boldsymbol{\nu}_t$ corresponds to measurement error. We are not concerned with inference on the non-dynamical error components here, thus a general specification of $\boldsymbol{\varepsilon}_t$ absorbs both types of error and simplifies the model. The process model in the reduced-dimensional space can then be written as,

$$\mathbf{a}_t = \mathbf{H}_t\mathbf{a}_{t-1} + \boldsymbol{\eta}_t, \text{ where } \boldsymbol{\eta}_t \sim N(\mathbf{0}, \mathbf{Q}), \text{ for } t = 1, \ldots, T. \tag{4}$$

The $l \times l$ matrix $\mathbf{H}_t$ can be thought of as a propagator matrix for the dynamical system at time t. Although this VAR (vector autoregressive) process is generally considered to be linear, in the case where the propagator matrix is time-varying it provides a simple way to build non-linear dynamics into the model. Although the process model in (4) is quite general, it would be difficult to estimate if allowed to vary at all times. However, seeking to study the dynamics of the system before and after year 1880, as well as how the dynamics change with drought conditions, we can simplify the model as follows (Wikle and Royle 2007):

$$\mathbf{a}_t = \begin{cases} \mathbf{H}_1\mathbf{a}_{t-1} + \boldsymbol{\eta}_t, & \text{if } t \le t^*, x_t < x^* \\ \mathbf{H}_2\mathbf{a}_{t-1} + \boldsymbol{\eta}_t, & \text{if } t \le t^*, x_t \ge x^* \\ \mathbf{H}_3\mathbf{a}_{t-1} + \boldsymbol{\eta}_t, & \text{if } t > t^*, x_t < x^* \\ \mathbf{H}_4\mathbf{a}_{t-1} + \boldsymbol{\eta}_t, & \text{if } t > t^*, x_t \ge x^*, \end{cases} \tag{5}$$

where $\mathbf{x} = \{x_1, \ldots, x_T\}'$ is the PDSI covariate (averaged over space) and x^* is a threshold above which indicates wet years and below which indicates dry years (in this case, $x^* = 0$). Recall that the year 1880 is a temporal changepoint, thus for the data considered here we let $t^* = 101$. In principle, one could allow t^* and x^* to be random variables in the hierarhical model, but that is not necessary here since inference is concerned with specific, known, values for these parameters.

The model in (5), which involves estimation of four fully random propagator matrices (along with all the other random parameters), is intuitive and easy to implement in a fully Bayesian setting. However, in our case where we only have a total of $T = 199$ times from which to estimate $4 \times l \times l$ parameters, may lead to an overfitted model. Since our focus is on the assessment of the propagator matrices, we want to have the highest reasonable data to parameter ratio (i.e., parsimonious model). Therefore, we consider the following reparameterization of the data and process models:

$$\mathbf{z}_t = \mathbf{y}_t + \boldsymbol{\varepsilon}_t, \boldsymbol{\varepsilon}_t \sim N(\mathbf{0}, \mathbf{R}), \tag{6}$$

$$\mathbf{y}_t = \begin{cases} \boldsymbol{\Phi}_1\mathbf{a}_t, \text{if } t \le t^* \\ \boldsymbol{\Phi}_2\mathbf{a}_t, \text{if } t > t^*, \end{cases} \tag{7}$$

$$\mathbf{a}_t = \begin{cases} \mathbf{H}_1\mathbf{a}_{t-1} + \boldsymbol{\eta}_t, & \text{if}, \quad x_t < x^*, \quad \boldsymbol{\eta}_t \sim N(\mathbf{0}, \mathbf{Q}_t) \\ \mathbf{H}_2\mathbf{a}_{t-1} + \boldsymbol{\eta}_t, & \text{if}, \quad x_t \ge x^*, \quad \boldsymbol{\eta}_t \sim N(\mathbf{0}, \mathbf{Q}_t), \end{cases} \tag{8}$$

where the basis functions $\boldsymbol{\Phi}_1$ and $\boldsymbol{\Phi}_2$ are found from the same decomposition as in (2) using $\mathbf{C}_0^1$ and $\mathbf{C}_0^2$, the sample lag-zero spatial covariance matrices from $\mathbf{z}_t$ with $t = 1, \ldots, t^* - 1$ and $t = t^*, \ldots, T$ respectively. This allows us to incorporate the temporal changepoint into the model while only having to estimate half as many propagator parameters. It can be shown that model (7) and (8) results in an implicit model similar to that of (5) in the space of $\mathbf{y}_t$ (for further details see Appendix A).

Now, consider the parameter models,

$$\mathbf{h}_1 = vec(\mathbf{H}_1) \sim N(\boldsymbol{\mu}_1, \boldsymbol{\Sigma}_1), \tag{9}$$

$$\mathbf{h}_2 = vec(\mathbf{H}_2) \sim N(\boldsymbol{\mu}_2, \boldsymbol{\Sigma}_2), \tag{10}$$

$$\mathbf{R}^{-1} \sim Wish((v_R\mathbf{C}_R)^{-1}, v_R), \tag{11}$$

and let $\mathbf{Q}_t$, the latent process error covariance, be defined as,

$$\mathbf{Q}_t = \sigma_Q^2 \mathbf{\Lambda}_t, \tag{12}$$

$$\mathbf{\Lambda}_t = \begin{cases} \mathbf{\Lambda}_1, & \text{if } t \leq t^* \\ \mathbf{\Lambda}_2, & \text{if } t > t^*, \end{cases} \tag{13}$$

$$\sigma_Q^2 \sim IG(r_Q, q_Q), \tag{14}$$

where $\mathbf{\Lambda}_1$ and $\mathbf{\Lambda}_2$ are the diagonal eigenvalue matrices resulting from the decomposition in (2). The vector $\mathbf{a}_0$ is the prior for the state vector at the time just before the data were observed and is distributed as $\mathbf{a}_0 \sim N(\boldsymbol{\mu}_0, \mathbf{\Sigma}_0 = \sigma_0^2 \mathbf{\Lambda}_1)$. Having little *a priori* intuition about the structure of the data model covariance ($\mathbf{R}$) indicates the need for a general prior such as the Wishart offers. Rather than impose spatial structure on the model, this specification accounts for our limited knowledge about the covariance while allowing for the possibility of spatial error structure.

Ultimately, we seek to make inference with the posterior distributions of our random parameters. i.e.,

$$[\mathbf{a}_{t=0,\ldots,T}, \mathbf{H}_1, \mathbf{H}_2, \mathbf{R}, \sigma_Q^2 | \mathbf{Z}, \mathbf{x}] \propto \prod_{t=1}^{T} [\mathbf{z}_t | \mathbf{a}_t, \mathbf{R}] \prod_{t \in \{t | x_t < x^*\}} [\mathbf{a}_t | \mathbf{a}_{t-1}, \mathbf{H}_1, \sigma_Q^2] \times \prod_{t \in \{t | x_t \geq x^*\}} [\mathbf{a}_t | \mathbf{a}_{t-1}, \mathbf{H}_2, \sigma_Q^2] [\mathbf{a}_0, \mathbf{H}_1, \mathbf{H}_2, \mathbf{R}, \sigma_Q^2]. \tag{15}$$

We make the assumption that the priors are independent, thus,

$$[\mathbf{a}_0, \mathbf{H}_1, \mathbf{H}_2, \mathbf{R}, \sigma_Q^2] \propto [\mathbf{a}_0][\mathbf{H}_1][\mathbf{H}_2][\mathbf{R}][\sigma_Q^2]. \tag{16}$$

Conjugate model specification and the assumption of independent priors allow for very efficient MCMC sampling. Although it may not be appropriate in all situations, the manner in which it is used here is quite flexible and robust, allowing, to a certain degree, for possible model misspecifications. More complex non-linear and non-conjugate hierarchical models are the focus of ongoing research.

Note that the joint posterior distribution and the relevant marginal distributions of interest are analytically intractable. Consequently, we use a Gibbs sampler to obtain samples from the posterior distribution. The full-conditional distributions used in the Gibbs sampler are given in Appendix B.

2.4 POP analysis

A useful method for assessing the structure of VAR dynamical systems is principal oscillation pattern (POP) analysis (Von Storch et al. 1995). As with EOF analysis, there are other ways to introduce POP analysis (i.e., as a model for the phenomena of interest) and although the continued use of compact matrix notation in what follows may seem terse, we emphasize that POP analysis in this setting is simply a matrix decomposition yielding very rich information about the evolution of ecological spatial patterns through time.

POP analysis involves a similar spectral decomposition as in (1) except now we decompose the propagator matrix (say $\mathbf{B}_k$, where k corresponds to different regimes) rather than the covariance matrix ($\mathbf{C}_0$). This cannot be approached in the same manner however, because $\mathbf{B}_k$, although square, may be non-symmetric ($\mathbf{B}_k \neq \mathbf{B}_k'$). In this setting, the characteristic

equation $|\mathbf{B}_k - \lambda\mathbf{I}|=0$ will have n roots (assuming $\mathbf{B}_k$ is $n \times n$), some of which may be complex. Consider the spectral decomposition:

$$\mathbf{B}_k = \mathbf{WDG}^*$$

where * denotes the Hermitian transpose (i.e., $\mathbf{G}^* = \bar{\mathbf{W}}^{-1}$, the inverse complex conjugate as in Caswell (2001)) and $\mathbf{W}$ is comprised of the right singular vectors $\{\mathbf{w}_1, \ldots, \mathbf{w}_n\}$ and $\mathbf{G}^*$ is comprised of the left singular vectors $\{\mathbf{g}_1^*, \ldots, \mathbf{g}_n^*\}$, $\mathbf{D} = diag(\delta_i)$ is diagonal, and $\mathbf{B}_k$ is the propagator matrix of the process: $\mathbf{y}_t = \mathbf{B}_k\mathbf{y}_{t-1} + \boldsymbol{\xi}_t$.

Inspection of the decomposition components can reveal much information about the stability and dynamical structure of the system (Von Storch et al. 1995). The vectors $\mathbf{w}_i$ are called the principal oscillation patterns (or system normal modes), while the elements of the vector $\boldsymbol{\alpha}_t$ are called the POP coefficients, where $\boldsymbol{\alpha}_t = \mathbf{G}^*\mathbf{y}_t$. In the spatio-temporal setting, $\mathbf{w}_j$ is a spatial map. The importance of this map to $\mathbf{y}_t$ is described by the magnitude of $\alpha_{j,t}$ when δ_j is real. In the event that δ_j is complex (i.e., $\delta_j = \delta_j^{\Re} + i\delta_j^{\Im}$, where $\Re$ and $\Im$ denote the real and imaginary components of the complex number respectively), δ_j has a sister root that is the complex conjugate of δ_j, say δ_k. Also note that we can write $\delta_j = \gamma_j e^{i\omega_j}$, where γ and ω are such that $\delta_j^{\Re} = \gamma_j \cos(\omega_j)$ and $\delta_j^{\Im} = \gamma_j \sin(\omega_j)$. Thus $\alpha_{j,t}$ evolves as a damped spiral in the complex plane with damping rate γ_j and frequency ω_j (when δ_j is complex and less than one in modulus).

The POP coefficients for the complex conjugate pair can be combined together and if we define $\mathbf{w}_j \equiv \mathbf{w}_j^{\Re} + i\mathbf{w}_j^{\Im}$, then the spatial pattern evolves throughout the period of oscillation as: $\ldots \to \mathbf{w}_j^{\Re} \to -\mathbf{w}_j^{\Im} \to -\mathbf{w}_j^{\Re} \to \mathbf{w}_j^{\Im} \to \mathbf{w}_j^{\Re} \to \cdots$ with a time interval of $\frac{\pi}{2\theta}$ between each successive pattern, where $\theta = \tan^{-1}\left(\frac{\delta_j^{\Re}}{\delta_j^{\Im}}\right)$. Additionally, if $|\delta_j| < 1$, the amplitude decreases exponentially and can be characterized by the "e-folding time" (the time needed to reduce the initial amplitude by e^1), $\tau_j = -1/\log(\gamma_j)$. Intuitively, when there exists a propagating wave in the state process, $\mathbf{w}^{\Im}$ is just a translated (in space) version of $\mathbf{w}^{\Re}$.

In the specific application considered here, we have two propagator matrices in the reduced dimension process model (8). A POP analysis on these propagator matrices would yield information about the dynamics in EOF space, not in a spatial context. To assess the changes in dynamics from a more intuitive perspective, we will consider a POP analysis on the implicit (full dimensional) process model:

$$\mathbf{y}_t = \begin{cases} \mathbf{B}_1\mathbf{y}_{t-1} + \boldsymbol{\xi}_t, & \text{if,} \quad x_t < x^*, t \le t^* \\ \mathbf{B}_2\mathbf{y}_{t-1} + \boldsymbol{\xi}_t, & \text{if,} \quad x_t \ge x^*, t \le t^* \\ \mathbf{B}_3\mathbf{y}_{t-1} + \boldsymbol{\xi}_t, & \text{if,} \quad x_t < x^*, t > t^* \\ \mathbf{B}_4\mathbf{y}_{t-1} + \boldsymbol{\xi}_t, & \text{if,} \quad x_t \ge x^*, t > t^*, \end{cases}$$

where, $\boldsymbol{\xi}_t = \boldsymbol{\Phi}_i\boldsymbol{\eta}_t$ and the $n \times n$ propagator matrices (as derived in Appendix A) are defined as,

$$\begin{aligned} \mathbf{B}_1 &\equiv \boldsymbol{\Phi}_1\mathbf{H}_1\boldsymbol{\Phi}_1', \\ \mathbf{B}_2 &\equiv \boldsymbol{\Phi}_1\mathbf{H}_2\boldsymbol{\Phi}_1', \\ \mathbf{B}_3 &\equiv \boldsymbol{\Phi}_2\mathbf{H}_1\boldsymbol{\Phi}_2', \\ \mathbf{B}_4 &\equiv \boldsymbol{\Phi}_2\mathbf{H}_2\boldsymbol{\Phi}_2'. \end{aligned}$$

Now, each propagator $\mathbf{B}_i$ will only yield l significant POPs due to the structure induced by the pre- and post-multiplication of the orthogonal basis functions. That is, the underlying dynam-

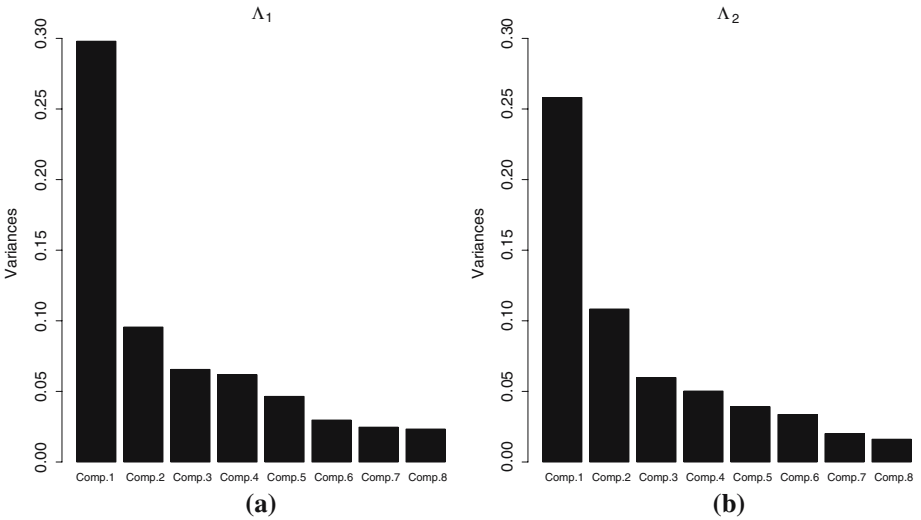

Fig. 2 Scree plots showing the proportion of variance (eigenvalues) explained by the orthogonal components of each decomposition. $\mathbf{\Lambda}_1$ from early years (pre-1880) and $\mathbf{\Lambda}_2$ from later years (post-1880)

ics exist on an l-dimensional manifold, but the expression of these dynamics in physical space is different for each period due to the different basis functions (projections).

3 Results

This section presents the results of fitting the model given in Sect. 2.3 to the data described in Sect. 2.1. The discussion of these results follows in Sect. 4.

Spectral decomposition of the spatio-temporal covariance matrix (2) from the data prior to and after the changepoint suggested that the correlation structure was indeed different for the two time periods (using $l = 4$, accounting for $> 80\%$ of the variability in data; scree plots of eigenvalues are in Fig. 2). This can be visually assessed by looking at the distribution of off-diagonal elements in the absolute difference of correlation matrices (corresponding to $\mathbf{C}_0^1$ and $\mathbf{C}_0^2$) for the two time periods (Fig. 3). In addition, a standard Bartlett's test for differences in covariance matrices confirmed that the two covariance structures are likely different, although this was only used as an exploratory measure for justifying the need for using two different sets of basis functions. Also of note is the correlation between the PDSI covariate and the principal components resulting from the EOF decompositions. The correlation between the first component and PDSI was approximately 0.5 while the correlation with the other components was less than 0.01 for both early (pre-1880) and late (post-1880) years.

The Gibbs sampler was run for 10,000 iterations with a burn-in period of 1,000 iterations and MCMC-based posterior statistics were calculated. Convergence was assessed visually using trace plots and occurred rapidly due in part to multivariate conjugate updates, identifiable model parameters, and relatively simple structure. The error term corresponding to the process model, σ_Q^2, has posterior mean and standard deviation of 0.224 and 0.048, respectively.

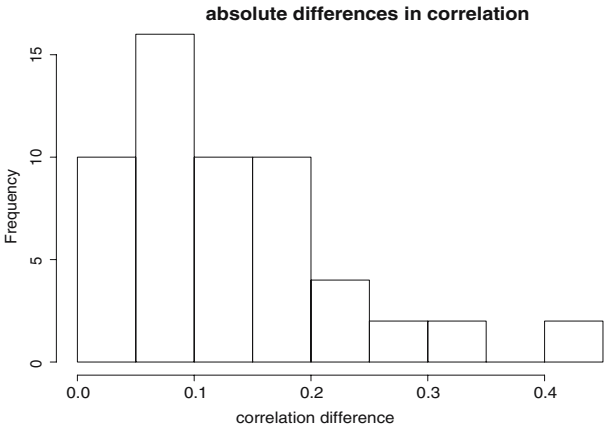

Fig. 3 Absolute differences in off-diagonal elements of the correlation matrices pre and post 1880

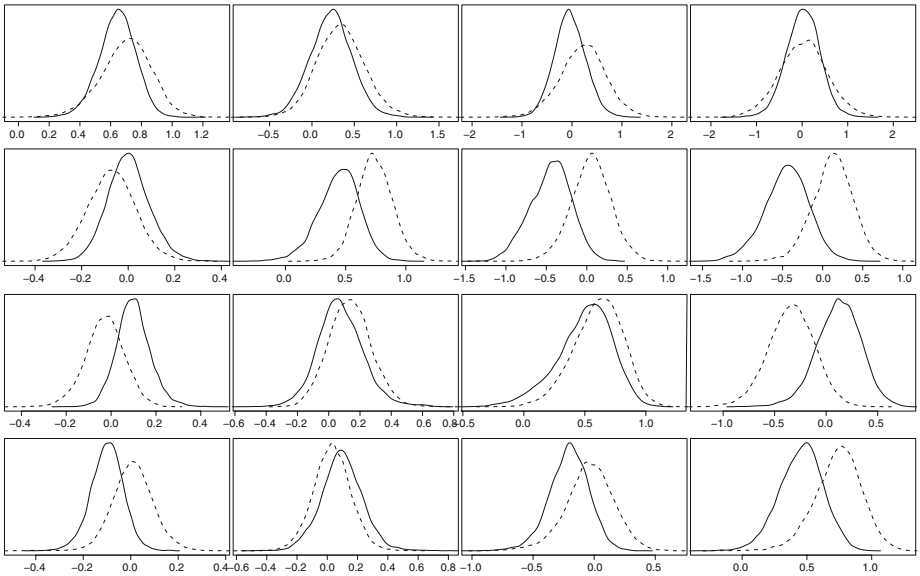

Fig. 4 Posterior distributions on an element by element basis for $\mathbf{H}_1$ (solid line, drought) and $\mathbf{H}_2$ (dashed line, non-drought). The arrangement of plots corresponds to the elements of the 4×4 propagator matrices from the process model (e.g., upper left plot represents the posterior distributions of element (1,1) from $\mathbf{H}_1$ and $\mathbf{H}_2$, etc)

The posterior distributions for the multivariate and matrix parameters in the model can be displayed in several ways. The posterior distributions for $\mathbf{H}_1$ and $\mathbf{H}_2$ can be viewed simultaneously to assess if (and how) they differ (Fig. 4). Consider also an image plot representing the posterior mean of the data model error covariance matrix $\mathbf{R}$ (Fig. 5). Also, since $\mathbf{a}_t, t = 1, \ldots, T$ consists of 199 times, it is best viewed as $l = 4$ individual time-series. The temporal dimension ($T = 199$) is too large to provide useful visual information here, thus we consider plots from a portion of each time-series (years 1827–1927) as a posterior mean

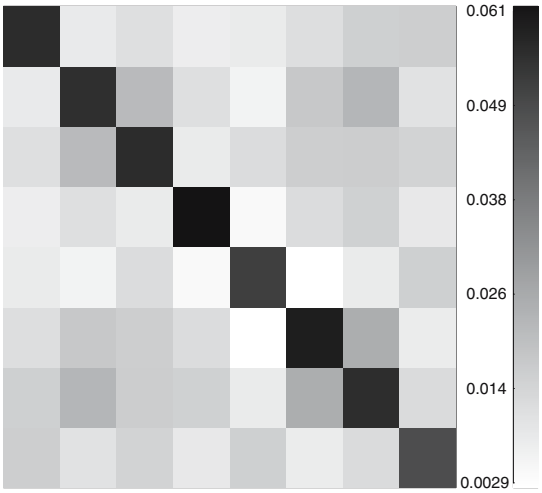

Fig. 5 Image representing the posterior mean of the error covariance matrix from the data model. Pixels in the image correspond to elements of the posterior mean matrix (i.e., $E([\mathbf{R}|\mathbf{Z}, \mathbf{x}])$

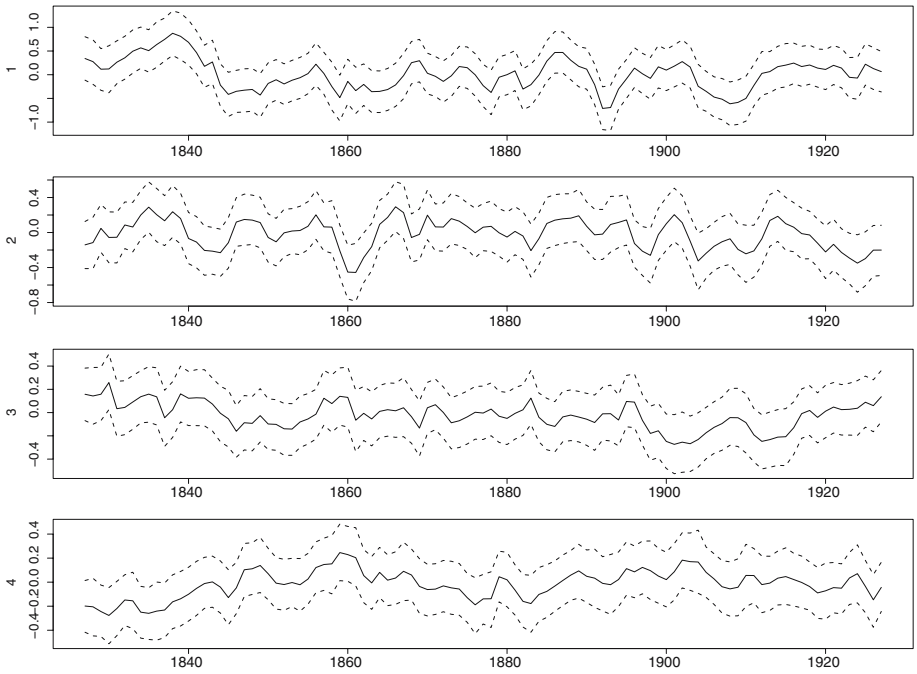

Fig. 6 Posterior means of the $\mathbf{a}_t$ process and 95% credible intervals for years 1827–1927

with 95% credible intervals (see Fig. 6). Additionally, we can view the posterior mean of the implicit propagator matrices ($\mathbf{B}_i$) as images (Fig. 7).

We can partially assess the dynamics of the system ($\mathbf{a}_t$, and hence the implicit process $\mathbf{y}_t$) by examining the POPs of the posterior mean $\mathbf{B}$ matrices. Table 2 summarizes the resulting eigenvalues from the POP decomposition (note, the eigenvalues for $\mathbf{B}_1$, $\mathbf{B}_3$ and $\mathbf{B}_2$, $\mathbf{B}_4$ must

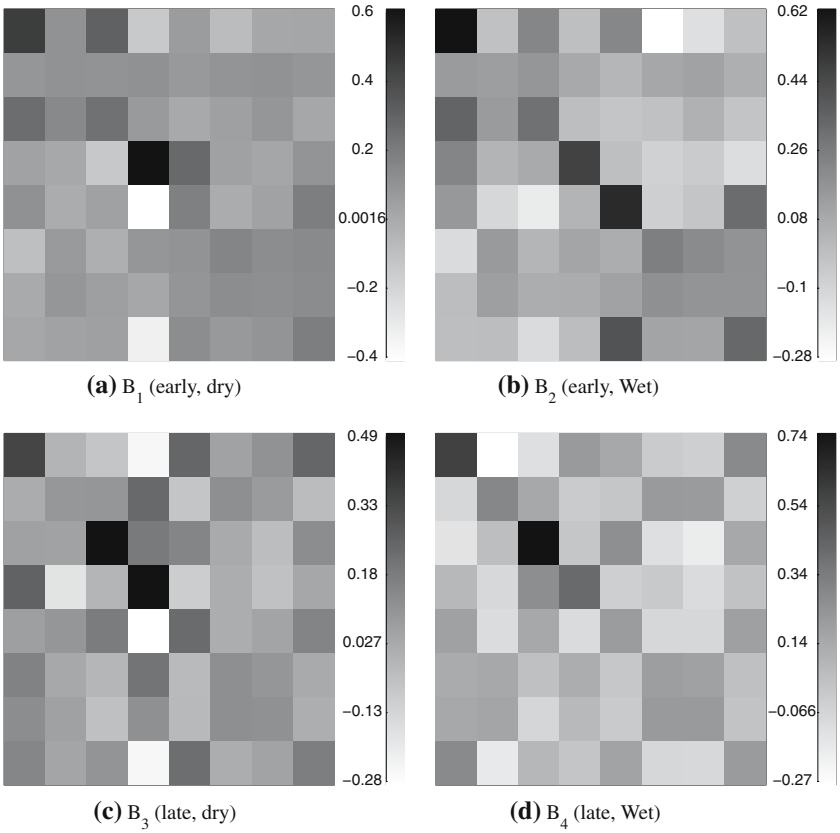

(a) B_1 (early, dry) **(b)** B_2 (early, Wet)

(c) B_3 (late, dry) **(d)** B_4 (late, Wet)

Fig. 7 Images representing the posterior mean of the implicit propagator matrices. Pixels in the images correspond to elements of the posterior mean matrices. Recall that the values in the ith row are weights relating the process at the previous time to the process in the ith location at the current time

Table 2 Significant eigenvalue summary from **B** matrices (complex eigenvalues are in the form $\delta = \delta^{\Re} + i\delta^{\Im}$)

$\mathbf{B}_1, \mathbf{B}_3$			$\mathbf{B}_2, \mathbf{B}_4$		
$\delta^{\Re}$	$\delta^{\Im}$	$\lvert\delta\rvert$	$\delta^{\Re}$	$\delta^{\Im}$	$\lvert\delta\rvert$
0.70	0	0.70	0.81	0	0.81
0.47	0.35	0.59	0.75	0.18	0.77
0.47	−0.35	0.59	0.75	−0.18	0.77
0.39	0	0.39	0.49	0	0.49

be the same since they correspond to the same reduced dimension propagators $\mathbf{H}_1$ and $\mathbf{H}_2$, respectively). Recall that the POPs can be viewed as spatial maps. Consider first the maps for the two POPs corresponding to real eigenvalues, POP_1 (Fig. 8) and POP_4 (Fig. 9).

Additionally, we present the complex POPs (corresponding to complex eigenvalues), as spatial maps that give some idea of the oscillating patterns. Figure 10 illustrates the oscillating nature of the system through the decomposition of the complex conjugate pair of POPs for each of the propagator matrices ($\mathbf{B}_i$).

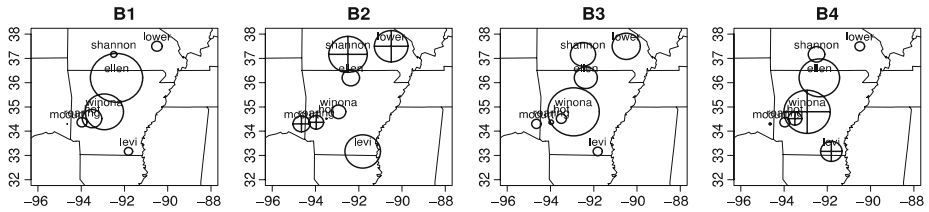

Fig. 8 The first normal mode plotted spatially for each of the **B** matrices. Open circles denote negative values, while circles with pluses represent positive values; larger circles imply larger magnitude, thus small circles are values near zero. From left to right: (early, dry), (early,wet), (late, dry), and (late, wet) years, respectively

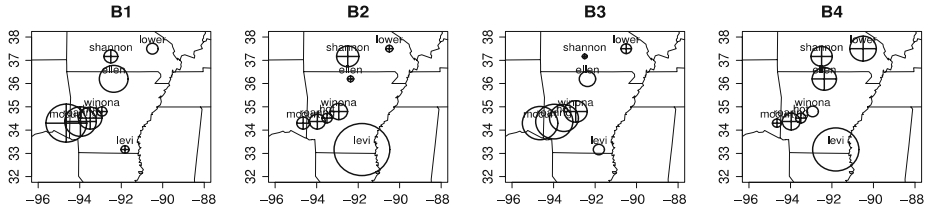

Fig. 9 The fourth normal mode plotted spatially for each of the **B** matrices. Open circles denote negative values, while circles with pluses represent positive values; larger circles imply larger magnitude, thus small circles are values near zero. From left to right: (early, dry), (early,wet), (late, dry), and (late, wet) years, respectively

The POP decomposition can also yield useful diagnostic measures. In this case, we can look at the frequencies, periods, and e-folding times. Table 3 presents the posterior estimates of these measures. Note that since the eigenvalues are the same, as in Table 2, we need only present two sets of estimates.

4 Discussion

Initial spectral decomposition of the data matrix ($\mathbf{Z}$) as in (2), revealed that $l = 4$ of the EOFs contributed greater than 80% of the variability in the data and provided a sufficient reduction in dimension to accomodate the dynamics of the system. Additionally, it was found that both of the matrices of basis functions in the data model (7) had dominant EOFs that were negatively associated with the covariate (PDSI) whereas EOF_2, EOF_3, and EOF_4 had little association with PDSI. This suggests that the most dominant component of the reduced latent process may be somewhat related to a response in growth due to drought. Based on the minimal associations of the remaining EOFs with PDSI these EOFs could correspond more with non-drought related factors (perhaps anthropogenic, biotic, and (or) other climatic factors). Despite any direct associations between the EOFs and PDSI covariate, it is possible for all elements of the process ($\mathbf{a}_t$) to evolve differently under different drought regimes. While other studies have focused on the more direct correlations of climate and tree growth, the emphasis here is on the dynamics of the tree growth over time as it relates to PDSI and anthropogenic influence. Figure 3 illustrates that regardless of EOF interpretation, differences in the lag-zero (in time) spatial correlation structure for the two time periods (i.e., before and after $t^* = 1880$) do exist. This implies that the EOFs will exhibit different behavior for the two time periods as well and indicates a need for two different sets of basis functions.

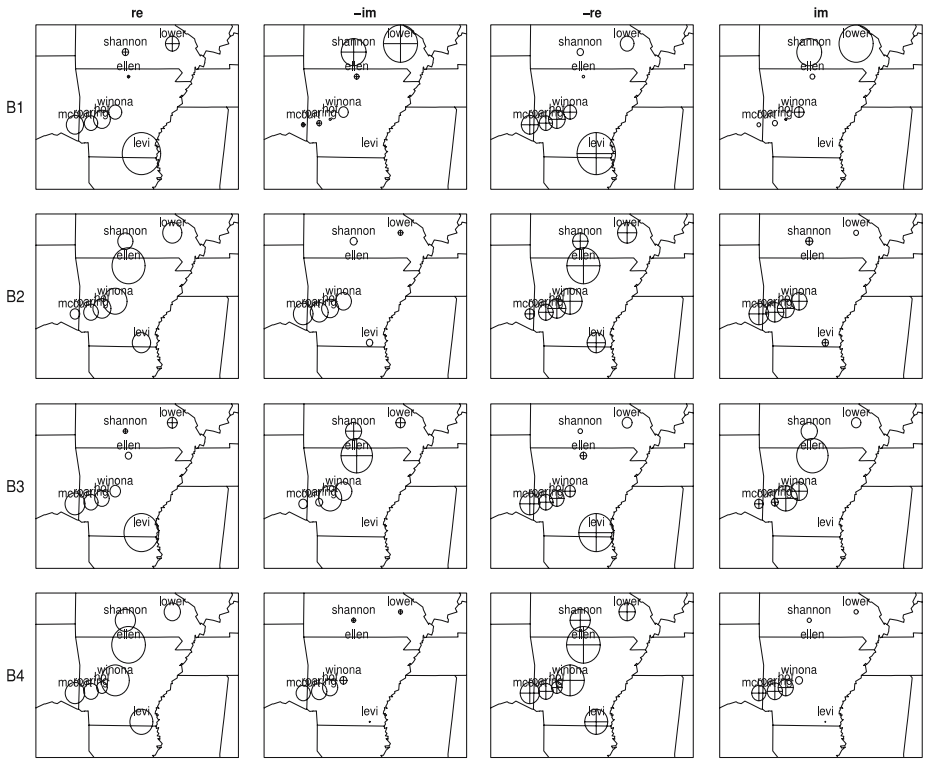

Fig. 10 The second (and third) normal mode plotted spatially for each of the **B** matrices. Open circles denote negative values, while circles with pluses represent positive values; larger circles imply larger magnitude, thus small circles are values near zero. Patterns evolve from left to right

Table 3 Frequencies, periods, and e-folding times from POP analysis of **B** matrices

$\mathbf{B}_1, \mathbf{B}_3$			$\mathbf{B}_2, \mathbf{B}_4$		
$\omega_j \left(\frac{\text{rad}}{\text{yr}}\right)$	$\frac{2\pi}{\omega_j} \left(\frac{\text{yrs}}{\text{cycle}}\right)$	τ_j (yr)	$\omega_j \left(\frac{\text{rad}}{\text{yr}}\right)$	$\frac{2\pi}{\omega_j} \left(\frac{\text{yrs}}{\text{cycle}}\right)$	τ_j (yr)
0.639	9.83	1.86	0.232	27.1	3.77

Values correspond to the complex pair of POPs (i.e., POP_2,POP_3)

It is important to note that these sets of basis functions ($\mathbf{\Phi}_1$, $\mathbf{\Phi}_2$) are not modeled in this setting. They only provide access to one of many latent systems and other sets of basis functions could be alternatively considered. In this case, they provide not only a means of dimension reduction, but also, basis functions typically act as decorrolaters, therefore a simple error structure ($\boldsymbol{\eta}_t$) on the latent process is reasonable. In general, projection of the data on a truncated EOF expansion acts as a filter and removes some of the noise in the data thereby magnifying the POP signal we wish to detect in the process model (Von Storch et al. 1995).

Inspection of the posterior mean of the error covariance matrix ($\mathbf{R}$) from the data model (Fig. 5) indicates that we are accounting for spatial auto-correlation in the data, as the posterior mean of ($\mathbf{R}$) contains spatial structure, some of which is likely due to the truncation error from (3) (Wikle and Cressie 1999; Beliner et al. 2000). Notice that data locations near each

other (e.g., locations 2 and 3) correspond to covariances (in **R**, Fig. 5) larger in magnitude than covariances corresponding to locations that are farther apart (e.g., locations 4 and 5).

The posterior mean and 95% credible interval for the $\mathbf{a}_t$ process in Fig. 6 illustrates the uncertainty associated with the latent dynamical system. Figure 4 illustrates the differences between the estimated propagator matrices that control the evolution of the latent process ($\mathbf{a}_t$). The differences in the posterior distributions of these propagators (i.e., $\mathbf{H}_1$ and $\mathbf{H}_2$) implies that the process evolves differently under drought conditions than it does during wetter years. A closer examination of the elements in $\mathbf{H}_1$ and $\mathbf{H}_2$ can reveal similarities and differences in the way the process evolves under varying conditions. Notice that the first row of plots in Figure 4 corresponds to the coefficients that form the linear combination of the elements in $\mathbf{a}_{t-1}$ to produce $a_{1,t}$. The first row suggests that there is little difference between propagator matrices in their influence on the first EOF, and really only the first two elements of $\mathbf{a}$ at the previous time ($t-1$) are important (i.e., non-zero) in this regard. However, the second row of plots highlights key differences in the propagator matrices. The second element of the process at the previous time is important in both drought and non-drought conditions, however the third and fourth elements at the previous time are likely only important to the process at the current time ($a_{2,t}$) during drought years. In the third row of plots, it is evident that $a_{1,t-1}$ is important to $a_{3,t}$ during drought years, while $a_{4,t-1}$ is important to $a_{3,t}$ only during non-drought years. A similar interpretation can be made with the fourth row of plots.

The disadvantage to interpreting these differences in the dynamics of the latent process is that we have little intuition about the components of this process themselves. We know that the first component (i.e., $a_{1,t}$) is somewhat related to the effect of PDSI on tree growth and that there are differences in the way the latent process evolves under varying drought regimes, but beyond that the components (EOFs or $\mathbf{a}_t$s) are difficult to interpret. They have the implicit spatial interpretation given by the eigenvectors of the EOF decomposition, however they lack any obvious anthropogenic, environmental, or biological meaning. We desire to assess the dynamics of the physical process (i.e., $\mathbf{y}_t$, tree growth) rather than the underlying process ($\mathbf{a}_t$) which evolves in a different and not always intuitive space.

Visualizing dynamical structure in the implicit process $\mathbf{y}_t$ may give us more insight on the scale of the observed process (i.e., the data). By viewing the posterior mean propagator matrices of the implicit process (Fig. 7) we can see how shortleaf pine growth at one location may be associated with growth at another location at the next time. Individually, these propagator matrices represent the implicit Markovian dynamics within each portion of the process subset by the time-period/covariate combinations. Thus we can more directly assess the changes in growth dynamics between drought and non-drought years before and after 1880.

Notice in Fig. 7 that the implicit propagator matrices corresponding to the covariate effect are similar. That is, $\mathbf{B}_1$ is similar to $\mathbf{B}_3$ (drought years) and $\mathbf{B}_2$ is similar to $\mathbf{B}_4$ (non-drought years), although not identical. This implies that the effect of PDSI on growth dynamics is more significant than change in time period. Subtle differences do exist however, between these similar propagator matrices. For example, the elements in the first row and third column of the matrices $\mathbf{B}_1$ and $\mathbf{B}_3$ are significantly different with a posterior mean difference of 0.37 and 95% credible interval of (0.08, 0.65). This suggests that during early years of drought ($\mathbf{B}_1$), shortleaf pine growth at the third location (winona) is positively associated with growth in the first location (ellen) at the next time. While after 1880, in drought years ($\mathbf{B}_3$), the eighth location (with posterior difference credible interval: $(-0.42, -0.01)$), rather than the the third location, is more associated with the first location at the next time. Similar spatio-temporal associations can be drawn between growth at various locations based on the interpretation of the different implicit propagator matrices. Such information is useful in cases where there

may be missing data and one might want to estimate the growth at a certain location and time given the rest of the data. Additionally, this can be useful in forcasting growth at various locations although the focus here is assessing the changes in growth dynamics.

Consider now a more formal method for evaluating the dynamics of the process. Spectral decomposition of the propagator matrices (non-symmetric) yields the principal oscillation patterns (or normal modes of the system). These POPs can be used to examine the oscillation properties and spatial structure of the implicit dynamical process ($\mathbf{y}_t$). Figure 8 illustrates that although the relative importance of the POPs themselves are the same for covariate-based groups (see Table 2), the normal modes are different, representing the varying dynamic structure in the process. This same information can be viewed spatially (Fig. 8). Notice that the first oscillation pattern for years when $x_t < x^*$ ($\mathbf{B}_1, \mathbf{B}_3$; drought years) is similar before and after 1880, but differs notably in the dynamics at two sites, ellen and winona. This implies that during drought years, the difference in dynamical structure accounted for by the first normal mode occurs at those sites. Likewise, for non-drought years, the dynamical structure evident in the first POP occurs between the two sites in southern Missouri (shannon and lower) and the site in southeast Arkansas (levi). Also of interest is the fact that the patterns corresponding to covariate effect are similar, suggesting that the response in growth to PDSI is more influential to the system (at least in the first normal mode of the system). As a contrast, consider the fourth POP (Fig. 9). In this normal mode, $\mathbf{B}_1$ and $\mathbf{B}_3$ are quite different from each other and different from $\mathbf{B}_2$ and $\mathbf{B}_4$ as well, although $\mathbf{B}_2$ and $\mathbf{B}_4$ are very similar. This implies that during drought years, the dynamics evident in the fourth mode are very different before and after 1880, however during non-drought years, there is little difference in the dynamics before and after 1880.

In the case where we have complex eigenvalues (POP_2 and POP_3), even more information is available about the oscillatory behavior of the system. Recall that the sequence of real and imaginary components from the complex pair of POPs corresponds to an evolving spatial pattern (Fig. 10) with frequency and period given in Table 3. These measures suggest that during drought years ($\mathbf{B}_1, \mathbf{B}_3$) the pattern sequence in the first and third row of Fig. 10 evolves more rapidly than the pattern in rows two and four (since the e-folding times are smaller in drought years). Notice again that the primary difference between time periods in drought years occurs at the ellen site, while in non-drought years the biggest difference in pattern occurs at the winona site. Another interesting feature is that in drought years the pattern evolves in a North/South fashion, while in wetter years, the pattern appears to evolve more in an East/West orientation.

5 Conclusion

The characterization of dynamical shifts in annual growth of shortleaf pine as a result of biotic and abiotic environmental factors as well as the biology of the species can be ecological and economically important from a management perspective. In order to thoroughly assess such shifts in vegetative dynamics in a given region, spatially explicit landscape scale data should be considered.

Such data, though readily available as dendrochronological (tree-ring) data, is subject to many sources of error. Additionally, the true process that generates the data (shortleaf pine growth) is likely correlated with changes in climate and other external influences as well as internal mechanisms that regulate growth over time. Such relationships coupled with a latent state-space process model can allow us to decompose and examine the underlying components driving the process. Here, we have adopted a model and model-output analysis

methods that allow us to determine if shifts in the system dynamics exist and characterize them in the presence of various sources of uncertainty (e.g., measurement and preprocessing error, spatial random effects, and possible model misspecifications).

Specifically, we show that by projecting the data (and implicit process in physical space) onto two reduced sets of basis functions corresponding to a changepoint in time (related to anthropogenic influence) we are able to implement a parsimonious model focused on accurate parameter estimation while implying a more complicated latent process model. Differences in the dynamical structure of shortleaf pine growth in the northwest portion of its natural range corresponding to levels of PDSI and time-period were found to be significant and therefore described in detail. Ecologists may find the spatially explicit properties of the posterior system dynamics useful for managing the species, especially in times of rapid climate change and (or) increasing anthropogenic influence.

The model and methods presented here, although new in this setting, have received much more popularity in fields where more obvious dynamical systems are present (e.g., fluid dynamics in atmospheric science and oceanography). High-dimensional spatio-temporal research is less common in ecological sciences due mostly to the difficulty in data collection. However, as more and more large scale datasets become available (such as those available from the International Tree-Ring Data Bank and the World Data Center for Paleoclimatology, as used here) more advanced methods common to other disciplines grow in utility for addressing ecological problems. Concerning the methods presented here, it is important to note that many other model specifications and parameterizations are possible and may be of varying utility in other applications.

Acknowledgements The authors would like to thank Richard P. Guyette and Michael C. Stambaugh for providing impetus for this project through their research (see references) and for providing useful information and suggestions about dendrochronological data. This research was funded by NSF Grant DMS 0139903.

Appendix A. Implicit process model

To show that model (7) and (8) imply an implicit model similar to (5), consider the process model:

$$\mathbf{a}_t = \begin{cases} \mathbf{H}_1\mathbf{a}_{t-1} + \boldsymbol{\eta}_t, & \text{if,} \quad x_t < x^*, \boldsymbol{\eta}_t \sim N(\mathbf{0}, \mathbf{Q}_t) \\ \mathbf{H}_2\mathbf{a}_{t-1} + \boldsymbol{\eta}_t, & \text{if,} \quad x_t \geq x^*, \boldsymbol{\eta}_t \sim N(\mathbf{0}, \mathbf{Q}_t), \end{cases} \tag{17}$$

and recall that,

$$\mathbf{y}_t = \begin{cases} \boldsymbol{\Phi}_1\mathbf{a}_t, & \text{if} \quad t \leq t^* \\ \boldsymbol{\Phi}_2\mathbf{a}_t, & \text{if} \quad t > t^*, \end{cases}$$

thus implying,

$$\Rightarrow \mathbf{a}_t = \begin{cases} \boldsymbol{\Phi}_1'\mathbf{y}_t, & \text{if} \quad t \leq t^* \\ \boldsymbol{\Phi}_2'\mathbf{y}_t, & \text{if} \quad t > t^*. \end{cases}$$

Then, substituting $\mathbf{\Phi}_i'\mathbf{y}_t$ into the LHS of model 17 we have,

$$\Rightarrow \begin{cases} \mathbf{\Phi}_1'\mathbf{y}_t = \begin{cases} \mathbf{H}_1\mathbf{a}_{t-1} + \boldsymbol{\eta}_t, & \text{if,} \quad x_t < x^*, \quad t \le t^* \\ \mathbf{H}_2\mathbf{a}_{t-1} + \boldsymbol{\eta}_t, & \text{if,} \quad x_t \ge x^*, \quad t \le t^* \end{cases} \\ \mathbf{\Phi}_2'\mathbf{y}_t = \begin{cases} \mathbf{H}_1\mathbf{a}_{t-1} + \boldsymbol{\eta}_t, & \text{if,} \quad x_t < x^*, \quad t > t^* \\ \mathbf{H}_2\mathbf{a}_{t-1} + \boldsymbol{\eta}_t, & \text{if,} \quad x_t \ge x^*, \quad t > t^*, \end{cases} \end{cases}$$

and pre-multiplying both sides by $\mathbf{\Phi}_i$ as well as substituting $\mathbf{\Phi}_i'\mathbf{y}_t$ into the RHS we have,

$$\Rightarrow \mathbf{y}_t = \begin{cases} \mathbf{\Phi}_1\mathbf{H}_1\mathbf{\Phi}_1'\mathbf{y}_{t-1} + \mathbf{\Phi}_1\boldsymbol{\eta}_t, & \text{if,} \quad x_t < x^*, \quad t \le t^* \\ \mathbf{\Phi}_1\mathbf{H}_2\mathbf{\Phi}_1'\mathbf{y}_{t-1} + \mathbf{\Phi}_1\boldsymbol{\eta}_t, & \text{if,} \quad x_t \ge x^*, \quad t \le t^* \\ \mathbf{\Phi}_2\mathbf{H}_1\mathbf{\Phi}_1'\mathbf{y}_{t-1} + \mathbf{\Phi}_2\boldsymbol{\eta}_t, & \text{if,} \quad x_t < x^*, \quad t = t^* + 1 \\ \mathbf{\Phi}_2\mathbf{H}_2\mathbf{\Phi}_1'\mathbf{y}_{t-1} + \mathbf{\Phi}_2\boldsymbol{\eta}_t, & \text{if,} \quad x_t \ge x^*, \quad t = t^* + 1 \\ \mathbf{\Phi}_2\mathbf{H}_1\mathbf{\Phi}_2'\mathbf{y}_{t-1} + \mathbf{\Phi}_2\boldsymbol{\eta}_t, & \text{if,} \quad x_t < x^*, \quad t > t^* + 1 \\ \mathbf{\Phi}_2\mathbf{H}_2\mathbf{\Phi}_2'\mathbf{y}_{t-1} + \mathbf{\Phi}_2\boldsymbol{\eta}_t, & \text{if,} \quad x_t \ge x^*, \quad t > t^* + 1. \end{cases}$$

Now, redefining the implicit propagator matrices of the system we have,

$$\Rightarrow \mathbf{y}_t = \begin{cases} \mathbf{B}_1\mathbf{y}_{t-1} + \boldsymbol{\xi}_t, & \text{if,} \quad x_t < x^*, \quad t \le t^* \\ \mathbf{B}_2\mathbf{y}_{t-1} + \boldsymbol{\xi}_t, & \text{if,} \quad x_t \ge x^*, \quad t \le t^* \\ \mathbf{B}_3^*\mathbf{y}_{t-1} + \boldsymbol{\xi}_t, & \text{if,} \quad x_t < x^*, \quad t = t^* + 1 \\ \mathbf{B}_4^*\mathbf{y}_{t-1} + \boldsymbol{\xi}_t, & \text{if,} \quad x_t \ge x^*, \quad t = t^* + 1 \\ \mathbf{B}_3\mathbf{y}_{t-1} + \boldsymbol{\xi}_t, & \text{if,} \quad x_t < x^*, \quad t > t^* + 1 \\ \mathbf{B}_4\mathbf{y}_{t-1} + \boldsymbol{\xi}_t, & \text{if,} \quad x_t \ge x^*, \quad t > t^* + 1. \end{cases}$$

where (recall that $\mathbf{Q}_i = \sigma_Q^2\mathbf{\Lambda}_i$),

$$\boldsymbol{\xi}_t = \begin{cases} \mathbf{\Phi}_1\boldsymbol{\eta}_t, & \text{if,} \quad t \le t^* \\ \mathbf{\Phi}_2\boldsymbol{\eta}_t, & \text{if,} \quad t > t^* \end{cases} \Rightarrow \boldsymbol{\xi}_t \sim \begin{cases} N(\mathbf{0}, \mathbf{\Phi}_1\mathbf{Q}_1\mathbf{\Phi}_1'), & \text{if,} \quad t \le t^* \\ N(\mathbf{0}, \mathbf{\Phi}_2\mathbf{Q}_2\mathbf{\Phi}_2'), & \text{if,} \quad t > t^* \end{cases}$$

$$\Rightarrow \boldsymbol{\xi}_t \sim \begin{cases} N(\mathbf{0}, \sigma_Q^2\mathbf{\Phi_1\Lambda_1\Phi_1'}), & \text{if,} \quad t \le t^* \\ N(\mathbf{0}, \sigma_Q^2\mathbf{\Phi_2\Lambda_2\Phi_2'}), & \text{if,} \quad t > t^* \end{cases} \Rightarrow \boldsymbol{\xi}_t \sim \begin{cases} N(\mathbf{0}, \sigma_Q^2\mathbf{C}_0^1), & \text{if,} \quad t \le t^* \\ N(\mathbf{0}, \sigma_Q^2\mathbf{C}_0^2), & \text{if,} \quad t > t^*. \end{cases}$$

Since we are only interested in the dynamics before and after the change point, then by allowing for two spatio-temporal covariance matrices in the data model, we have an implicit model on the $\mathbf{y}_t$'s (for $t = 1, \ldots, t^*, t^* + 2, \ldots, T$) with 4 (or more) propagator matrices:

$$\Rightarrow \mathbf{y}_t = \begin{cases} \mathbf{B}_1\mathbf{y}_{t-1} + \boldsymbol{\xi}_t, & \text{if,} \quad x_t < x^*, \quad t \le t^* \\ \mathbf{B}_2\mathbf{y}_{t-1} + \boldsymbol{\xi}_t, & \text{if,} \quad x_t \ge x^*, \quad t \le t^* \\ \mathbf{B}_3\mathbf{y}_{t-1} + \boldsymbol{\xi}_t, & \text{if,} \quad x_t < x^*, \quad t > t^* \\ \mathbf{B}_4\mathbf{y}_{t-1} + \boldsymbol{\xi}_t, & \text{if,} \quad x_t \ge x^*, \quad t > t^*. \end{cases}$$

□

Appendix B. Full-conditionals

To streamline the notation let,

$$\mathbf{\Phi}_t = \begin{cases} \mathbf{\Phi}_1, & \text{if} \quad t = 1, \ldots, t^* - 1 \\ \mathbf{\Phi}_2, & \text{if} \quad t = t^*, \ldots, T, \end{cases}$$

$$\mathbf{H}_t = \begin{cases} \mathbf{H}_1, & \text{if} \quad t \in \{t | x_t < x^*\} \\ \mathbf{H}_2, & \text{if} \quad t \in \{t | x_t \geq x^*\}, \end{cases}$$

This allows us to write the posterior distribution as:

$$[\mathbf{a}_{t=0,\ldots,T}, \mathbf{H}_1, \mathbf{H}_2, \mathbf{R}, \sigma_Q^2 | \mathbf{Z}, \mathbf{x}] \propto \prod_{t=1}^{T} [\mathbf{z}_t | \mathbf{a}_t, \mathbf{R}] \prod_{t=1}^{T} [\mathbf{a}_t | \mathbf{a}_{t-1}, \mathbf{H}_t, \sigma_Q^2] \times [\mathbf{a}_0][\mathbf{H}_1][\mathbf{H}_2][\mathbf{R}][\sigma_Q^2].$$

Thus we can write the full-conditional distributions as:

$$\begin{aligned}
\mathbf{a}_0 | \cdot &\sim N((\mathbf{H}_1' \mathbf{Q}_1^{-1} \mathbf{H}_1 + \mathbf{\Sigma}_0^{-1})^{-1} (\mathbf{H}_1' \mathbf{Q}_1^{-1} \mathbf{a}_1 + \mathbf{\Sigma}_0^{-1} \boldsymbol{\mu}_0), (\mathbf{H}_1' \mathbf{Q}_1^{-1} \mathbf{H}_1 + \mathbf{\Sigma}_0^{-1})^{-1}), \\
\mathbf{a}_t | \cdot &\sim N((\mathbf{\Phi}_t' \mathbf{R}^{-1} \mathbf{\Phi}_t + \mathbf{Q}_t^{-1} + \mathbf{H}_{t+1}' \mathbf{Q}_{t+1}^{-1} \mathbf{H}_{t+1})^{-1} (\mathbf{\Phi}_t' \mathbf{R}^{-1} \mathbf{z}_t + \mathbf{Q}_t^{-1} \mathbf{H}_t \mathbf{a}_{t-1} \\
&\quad + \mathbf{H}_{t+1}' \mathbf{Q}_{t+1}^{-1} \mathbf{a}_{t+1}), (\mathbf{\Phi}_t' \mathbf{R}^{-1} \mathbf{\Phi}_t + \mathbf{Q}_t^{-1} + \mathbf{H}_{t+1}' \mathbf{Q}_{t+1}^{-1} \mathbf{H}_{t+1})^{-1}), \\
&\quad \text{for } t = 1, \ldots, T-1, \\
\mathbf{a}_T | \cdot &\sim N((\mathbf{\Phi}_T' \mathbf{R}^{-1} \mathbf{\Phi}_T + \mathbf{Q}_T^{-1})^{-1} (\mathbf{\Phi}_T' \mathbf{R}^{-1} \mathbf{z}_T + \mathbf{Q}_T^{-1} \mathbf{H}_T \mathbf{a}_{T-1}), \\
&\quad (\mathbf{\Phi}_T' \mathbf{R}^{-1} \mathbf{\Phi}_T + \mathbf{Q}_T^{-1})^{-1}), \\
\mathbf{h}_i | \cdot &\sim N(\mathbf{V}_i^{-1} \mathbf{b}_i, \mathbf{V}_i^{-1}), \quad \text{for} \quad i = 1, 2, \\
\mathbf{R}^{-1} | \cdot &\sim Wish \left(\left(\sum_{t=1}^{T} (\mathbf{z}_t - \mathbf{\Phi}_t \mathbf{a}_t)(\mathbf{z}_t - \mathbf{\Phi}_t \mathbf{a}_t)' + v_R \mathbf{C}_R \right)^{-1}, v_R + T \right), \\
\sigma_Q^2 | \cdot &\sim IG \left(\left(\frac{1}{2} \sum_{t=1}^{T} (\mathbf{a}_t - \mathbf{H}_t \mathbf{a}_{t-1})' \mathbf{\Lambda}_t^{-1} (\mathbf{a}_t - \mathbf{H}_t \mathbf{a}_{t-1}) + \frac{1}{r_Q} \right)^{-1}, \frac{lT}{2} + q_Q \right).
\end{aligned}$$

Defining the index sets as $M_1 = \{t | x_t < x^*\}$ and $M_2 = \{t | x_t \geq x^*\}$ with $m_1 = dim(M_1)$ and $m_2 = dim(M_2)$, we have:

$$\mathbf{V}_i = (\mathbf{A}_{m_i - 1}' \otimes \mathbf{I}_l)' \tilde{\mathbf{Q}}_i^{-1} (\mathbf{A}_{m_i - 1}' \otimes \mathbf{I}_l) + \mathbf{\Sigma}_i^{-1}$$

$$\mathbf{b}_i = (\mathbf{A}_{m_i - 1}' \otimes \mathbf{I}_l)' \tilde{\mathbf{Q}}_i^{-1} vec(\mathbf{A}_{m_i}) + \mathbf{\Sigma}_i^{-1} \boldsymbol{\mu}_i$$

where,

$$\begin{aligned}
\mathbf{A}_{m_i} &\equiv [(\mathbf{a}_t)]_{l \times m_i}, \quad t \in M_i \\
\mathbf{A}_{m_i - 1} &\equiv [(\mathbf{a}_{t-1})]_{l \times m_i}, \quad t \in M_i \\
\tilde{\mathbf{Q}}_i &\equiv blockdiag(\mathbf{Q}_t), \quad t \in M_i.
\end{aligned}$$

References

Ash R (1975) Topics in stochastic processes. Academic Press
Beliner L, Wikle C, Cressie N (2000) Long-lead prediction of Pacific SSTs via bayesian dynamic modeling. J Climate 13:3953–3968
Berliner L (1996) In: Maximum Entropy and Bayesian Methods, Chapter hierarchical Bayesian time series models, p 15–22. Kluwer Academic Publishers
Caswell H (2001) Matrix population models: construction, analysis, and interpretation. Sinauer Associates, Inc, Sunderland, Massachusetts
Contributors of the International Tree-Ring Data Bank (2005) IGBP PAGES/World Data Center for Paleoclimatology, NOAA/NCDC Paleoclimatology Program; Boulder, Colorado
Cook E, Holmes R (1986) Users manual for Program ARSTAN. Laboratory of Tree-Ring Research, University of Arizona, Tuscon, Arizona
Cook E, Meko D, Stahle D (1999) Drought reconstructions for the continental United States. J Climate 12: 1145–1162
Cunningham R, Hauser C (1989) The decline of Missouri forests between 1880 and 1920. Pages 34–37 In: Walldrop T (ed) Proceedings of pine-hardwood mixtures: a symposium on the management and ecology of the type, volume GTR. US Department of Agriculture, Forest Service, Southeastern Forest Experiment Station, Asheville, North Carolina
Fritts H (1976) Tree rings and climate. Academic Press, New York
Guyette R, Muzika R, Dey D (2002) Dynamics of an anthropogenic fire regime. Ecosystems 5:472–486
Hamilton J (2003) Historic and contemporary vegetation/environment relationships in the shortleaf pine region of the Missouri Ozarks. Master's Thesis, University of Missouri, Columbia, Missouri, USA
Papoulis R, Pillai S (2002) Probability, random variables, and stochastic processes. McGraw-Hill
Preisendorfer R (1988) Principal component analysis in meteorology and oceanography. Elsevier
Stambaugh M (2001) Forest canopy gap disturbances in shortleaf pine forests of the Ozark highlands. Master's Thesis, University of Missouri, Columbia, Missouri, USA
Stambaugh M, Guyette R (2004) Long-term growth and climate response of Shortleaf Pine at the Missouri Ozark Forest Ecosystem Project. Proceedings of the 14th Central Hardwood Forest Conference pages 448–458
Stokes M, Smiley T (1996) An introduction to tree ring dating. University of Arizona Press, Tuscon, Arizona
Von Storch H, Burger G, Schnur R, Von Storch J (1995) Principal oscillation patterns: a review. J Climate 8: 377–400
Wikle C, Cressie N (1999) A dimension reduced approach to space-time Kalman filtering. Biometrika 86: 815–829
Wikle C, Royle J (2007) Predicting migratory bird settling patterns with hierarchical Bayesian spatio-temporal models. In Review

Author sketches

Mevin B. Hooten earned BS and MS degrees from Kansas State University in Natural Resources (1999) and the University of Missouri – Columbia in Forestry (2001), respectively. He then obtained a PhD in Statistics (2006) from the University of Missouri – Columbia, with dissertation research focusing on hierarchical spatio-temporal statistical models for ecological processes. He is currently an Assistant Professor of Statistics in the Department of Mathematics and Statistics, a Faculty Associate of the Ecology Center, and an Adjunct Faculty Member in the Department of Wildland Resources at Utah State University. His research interests are in the development and application of spatial, temporal, and spatio-temporal models for natural systems and the interface between applied mathematics and statistics.

Christopher K. Wikle obtained BS and MS degrees in atmospheric science from the University of Kansas in 1986 and 1989, respectively. From 1988 to 1991 he worked as an air pollution consultant, primarily studying potential environmental impacts of proposed power generation facilities. He then obtained an MS in statistics at Iowa State University in 1994 and a co-major PhD in both atmospheric science and statistics at Iowa State University in 1996. From 1996 to 1998 he was a visiting scientist in the Geophysical Statistics Project at the National Center for Atmospheric Research in Boulder, Colorado. He is currently Associate Professor of Statistics and Adjunct Professor of Atmospheric Science at the University of Missouri, Columbia. He was elected Fellow of the American Statistical Association in 2004. His research interests are in the application

of statistics to geophysical and environmental processes. Specific interests include spatio-temporal models, hierarchical Bayesian methods, the introduction of physical information into stochastic models, statistical design of environmental monitoring networks, climate dynamics, atmospheric waves, nowcasting, ecology, and models for invasive species.